ELSEVIER

Biochimica et Biophysica Acta 1285 (1996) 131–145

BBA

The mechanism of monensin-mediated cation exchange based on real time measurements

E. Nachliel, Y. Finkelstein [1], M. Gutman *

Laser Laboratory for Fast Reactions in Biology, Department of Biochemistry, George S. Wise Faculty of Life Sciences, Tel Aviv University, Ramat Aviv 69978, Israel

Received 15 May 1996; revised 19 July 1996; accepted 19 July 1996

Abstract

Monensin is an ionophore that supports an electroneutral ion exchange across the lipid bilayer. Because of this, under steady-state conditions, no electric signals accompany its reactions. Using the Laser Induced Proton Pulse as a synchronizing event we selectively acidify one face of a black lipid membrane impregnated by monensin. The short perturbation temporarily upsets the acid–base equilibrium on one face of the membrane, causing a transient cycle of ion exchange. Under such conditions the molecular events could be discerned as a transient electric polarization of the membrane lasting approx. 200 μs. The proton-driven chemical reactions that lead to the electric signals had been reconstructed by numeric integration of differential rate equations which constitute a maximalistic description of the multi equilibria nature of the system (Gutman, M. and Nachliel, E. (1989) Electrochim. Acta 34, 1801–1806). The analysis of the reactions reveals that the ionic selectivity of the monensin ($H^+ > Na^+ > K^+$) is due to more than one term. Besides the well established different affinity for the various cations, the selectivity is also derived from a large difference in the rates of cross membranal diffusivities (MoH > MoNa > MoK), which have never been detected before. (v) Quantitative analysis of the membrane's crossing rates of the three neutral complexes reveals a major role of the membranal dipolar field in regulating ion transport. The diffusion of MoH, which has no dipole moment, is hindered only by the viscose drag. On the other hand, the dipolar complexes (MoNa and MoK) are delayed by dipole–dipole interaction with the membrane. (vi) Comparison of the calculated dipoles with those estimated for the crystalline conformation of the $[MoNa(H_2O)_2]$ and $[MoK(H_2O)_2]$ complexes reveals that the MoNa may exist in the membrane at its crystal configuration, while the MoK definitely attains a structure having a dipole moment larger than in the crystal.

Keywords: Monensin; Proton–cation exchange; Viscosity; Dipolar field; Time-resolved polarization; Polarization; Ionic selectivity

1. Introduction

Monensin is an extensively studied ionophore which has been in use as a biochemical tool for almost 30 years [1]. Its three dimensional structure, in complex with many cations, is well-known [2–4] and the atomic coordinates are retrievable. The compound is a five ring structure (see Scheme 1) which wraps

Abbreviations: PC, phosphatidylcholine; PS, phosphatidylserine; MoM, monensin-metal complex; MoH, protonated monensin; ϕOH, ϕO^-, 8-hydroxypyrene 1,3,6-trisulfonate in its protonated and ionized state, respectively.

* Corresponding author. Fax: +972 3 6415053.

[1] Present address: Department of Physics, Ben Gurion University of the Negev, Beersheba, Israel.

PII S0005-2736(96)00149-6

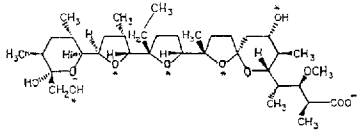

Scheme 1. Molecular structure of monensin. The atoms marked by (*) are the ligand of the metal ion. Please note that the carboxylate is not involved.

the metal cation in a configuration that does not employ the single carboxylate as a ligand. As a result all metallic ion monensin complexes, though neutral, retain a dipole moment. The proton is the only cation that reacts directly with the carboxylate.

The ionophoric function of monensin is attributed to the membrane solubility of the two neutral complexes: monensin-metal (MoM) and protonated monensin (MoH). The general scheme of its operation [1] assumed that each form diffuses independently across the membrane, equilibrates with the prevailing ions and by back diffusion brings an ionic equilibration between the bathing solution on the two sides of the membrane. More recent experiments by Prabhananda and Kombrabail [5] employed a T-jump technique for rapid acidification of solution. Their analysis of time-resolved measurements considered the MoH and

D side		membrane	R side
$\Phi CH \overset{k_2}{\underset{k_1}{\rightleftharpoons}} \Phi O^- + H^-$		(1)	
$P_S + H^- \overset{k_{11}}{\underset{k_{12}}{\rightleftharpoons}} P_SH$		(2)	
$Mo^- + H^- \overset{k_3}{\underset{k_4}{\rightleftharpoons}} MoH$		(3)	
$MoNa + H^- \overset{k_5}{\underset{k_6}{\rightleftharpoons}} MoNaH^+$		(4)	
$Mo^- + P_SH \overset{k_{36}}{\underset{k_{35}}{\rightleftharpoons}} MoH + P_S^-$		(5)	
$P_SH + MoNa \overset{k_{38}}{\underset{k_{37}}{\rightleftharpoons}} P_S^- + MoNaH^+$		(6)	
$MoNa + MoH \overset{k_{40}}{\underset{k_{39}}{\rightleftharpoons}} MoNaH^+ + Mo^-$		(7)	
$MoH + \Phi O^- \overset{k_{31}}{\underset{k_{32}}{\rightleftharpoons}} Mo^- + \Phi OH$		(8)	
$P_SH + \Phi O^- \overset{k_{33}}{\underset{k_{34}}{\rightleftharpoons}} P_S^- + \Phi OH$		(9)	
$MoNaH^+ \overset{k_5}{\underset{k_6}{\rightleftharpoons}} Na^+ + MoH$		(10)	
$MoNa \overset{k_{10}}{\underset{k_9}{\rightleftharpoons}} Na^+ + Mo^-$		(11)	
MoH		$\overset{20}{\underset{21}{\rightleftharpoons}}$	MoH (12)
MoNa		$\overset{22}{\underset{29}{\rightleftharpoons}}$	MoNa (13)
		(2)	$P_S^- + H^- \overset{k_{11}}{\underset{k_{12}}{\rightleftharpoons}} P_SH$
		(3)	$Mo^- + H^- \overset{k_3}{\underset{k_4}{\rightleftharpoons}} MoH$
		(4)	$MoNa + H^- \overset{k_5}{\underset{k_6}{\rightleftharpoons}} MoNaH^+$
		(5)	$Mo^- + P_SH \overset{k_{36}}{\underset{k_{35}}{\rightleftharpoons}} MoH + P_S^-$
		(6)	$P_SH + MoNa \overset{k_{38}}{\underset{k_{37}}{\rightleftharpoons}} P_S^- + MoNaH^+$
		(7)	$MoNa + MoH \overset{k_{40}}{\underset{k_{39}}{\rightleftharpoons}} MoNaH^+ + Mo^-$
		(10)	$MoNaH^+ \overset{k_5}{\underset{k_6}{\rightleftharpoons}} Na^+ + MoH$
		(11)	$MoNa \overset{k_{10}}{\underset{k_9}{\rightleftharpoons}} Na^+ + Mo^-$

Scheme 2. Listing of all chemical equilibria that were incorporated in the numeric simulation of the reaction. On the left side (driving compartment) protons are discharged by the laser pulse (reaction 1). The discharged protons upset the acid-base equilibria of the phosphoserine headgroups (2), the monensin anion (3) and the MoNa complex (4). Reactions 5, 6 and 7 are proton transfer reactions between the component on the membrane. The reaction of ΦO^-, acting as a base, with membranal components, are given by reactions 8 and 9. The flux of MoH and MoNa are defined by reactions 12 and 13. The forward and backward rates for each species are identical (i.e. $k_{20} = k_{21}$). The reactions on the right side (responsive) compartment are identical to those on the D face except that the pyranine is not present on that side.

MoM complexes as diffusing species, while a ternary complex ($MoNaH^+$), formed during the reaction, was taken as a dead-end product. This assumption is in contradiction to the equilibrium measurements of Cox et al. [6] which place the ternary complex formation as a key reaction for the overall exchange mechanism. According to Cox, the binding of a proton to the carboxylate of MoM reduces the affinity for the metal ion with its subsequent ejection to the bulk. This mechanism stimulated us to exploit the Laser Induced Proton Pulse as a synchronizing event for studying the monensin mediated H^+/Na^+ exchange in the time-resolved domain [7].

In our experiments the ionophore, impregnated in a black lipid membrane, was subjected to pulse protonation by photoexcitation of pyranine (8-hydroxypyrene 1,3,6-trisulfonate) added exclusively on one side of the membrane. The discharged protons converted the MoNa complex to the ternary one, which decomposed to MoH and Na^+, perturbing the equilibrium of the neutral complexes between the two faces of the membrane. The perturbation was then propagated across the membrane (see Scheme 2) via the counter diffusion of the two neutral complexes, causing the H^+ and Na^+ exchange to take place. Due to the high resolution of the monitoring system and the high synchronism of the perturbation, the electrosilence of H^+/Na^+ exchange was broken and an electric signal was recorded.

In a previous study [7] we formulated the chemical events that lead to the appearance of the electric transient. For that purpose we grouped all reactions associated with the perturbation (see Scheme 2) into an array of chemical equilibria proceeding on both sides of the membrane (see left and right side of the scheme) and converted them into a set of coupled, non linear differential rate equations which comply with the detailed balance principle. Upon integration of these equations, and using the rate constants as adjustable parameters, we were able to reproduce with high accuracy the electric signal measured at a given NaCl concentration. The present study is an expansion of the analytic procedure which is applied on a large set of experimental tracings, where the metal ion (either Na^+ or K^+) concentrations span the whole saturation curve of the ionophore. The analysis of many independent experimental curves increased the accuracy of the calculated rate constants and provided us with a tool for studying the ionic selectivity of the monensin.

Past studies attributed the enhanced flux of Na^+ vs. K^+ to the higher stability of the MoNa complex while dynamic considerations, like unequal rates of diffusion, were a priori ignored [1,5]. The fact that the mass and dimensions of MoH, MoNa and MoK are comparable naturally led to the approximation that they will cross the membrane at equal rates. The high time resolution of our experiments, and the precision of the numeric analysis, revealed that the diffusivities of the three uncharged species are not equal.

The different diffusivities of the neutral complexes of the monensin are derived from their molecular structure. The MoH complex, where the proton binds to the carboxylate [2–4] is chargeless and bears no dipole moment, therefore its diffusion will be affected only by the membrane's viscosity. The two metallic complexes are neutral in charge but due to the fact that the carboxylate is not a binding ligand for the ion, they bear a finite dipole moment. The permanent dipole of these molecules interacts with the dipolar field of the membrane [8,9] adding an electric barrier on top of the viscose drag. Consequently both MoNa and MoK should have smaller diffusivities than MoH. Our measurements confirmed this prediction.

Comparison of the dipole moment of MoNa, as deduced from its diffusivity, indicates that its structure at the water/membrane interface may be identical to the crystalline structure, in accord with the observation that its solution conformation (in $CHCl_3$) is similar to its crystal configuration [10]. On the other hand the MoK in the membrane has a configuration that is not compatible with the crystal structure.

2. Materials and methods

Phospholipids (phosphatidylcholine and phosphatidylserine) were purchased from Avanti Polar Lipids (Alabaster, AL, USA).

Monensin and choline chloride were Sigma products (St. Louis, MO, USA). Pyranine (8-hydroxypyrene 1,3,6-trisulfonate) laser grade was supplied by Eastman Kodak (Rochester, NY, USA).

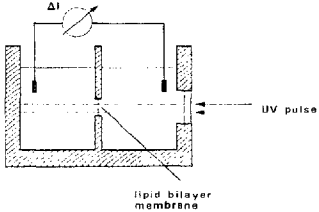

Scheme 3. Schematic representation of the experimental setup. The black lipid membrane is built on a 1 mm pore separating two compartments (7 ml each) in a cell equipped with a quartz window through which the laser pulse irradiates the membrane. The beam (having a diameter of ≈ 0.2 mm) does not irradiate the torus of the membrane. The proton emitting dye, pyranine, is added on the back compartment so that the energy of the beam is not attenuated until it approaches the D face of the membrane. The capacitance current is picked up by two black platinum electrodes which are shielded from the light by plastic sleeves. The current was measured by a current voltage converters (10^7 V/A) made in the Electronic Workshop of the Max Planck Institute for Biophysics, Frankfurt and in the Electronic Workshop of the School of Chemistry, Tel Aviv University.

The photo excitation of pyranine was induced by the third harmonic frequency (355 nm) of a Nd Yag laser. The pulses (2 ns full width at half-maximum (FWHM)) were attenuated by glass filters to energy of approx. 0.25 mJ/pulse and focused on the black lipid membrane covering the orifice of the observation cell. The diameter of the irradiated spot was about 0.2 mm.

The observation cell was made (see Scheme 3) with an orifice of 1 mm in diameter connecting the two troughs, each containing 7 ml of 0.1 M choline chloride, buffered by 50 μM Mes to pH = 5.7. Pyranine 150 μM was added to the back trough: this side of the membrane will be referred to as the driving (D) side. Capacitance currents were picked up by the black platinum coated Pt electrodes. The electrodes were shielded from light by black plastic sleeves. The current was monitored by a current–voltage converter having a 50 MHz band width with an output of 10^7 V/A. The impedance of the measuring circuit was about 2000 Ω. This value is negligible with respect to the resistance of the membrane (≈ 1 GΩ). The signals were collected, digitized and stored by a Tektronix 2430A digital oscilloscope.

Black lipid membranes (BLM) were built up by first impregnating the dry septum of the observation cell by 5 μl of 0.5% phospholipids (PS/PC = 2:3, w/w) dissolved in hexane. After evaporation of the solvent by a stream of dry nitrogen, the cell was filled with the choline chloride-Mes solution, placed on rack within a Faraday cage and 5 μl of 1.5% phospholipid dissolved in decane were added to the orifice to make a membrane. The membrane became black within 15 min and had a capacitance of about 2 nF. The membrane was stable for at least 3–4 h. Each set of experiments was carried out with the very same membrane. During measurements the content of each compartment was stirred constantly.

In a typical experiment we first verified the capacitance of the membrane, then the membrane was equilibrated against 20 μM monensin added (in ethanolic solution) to both sides of the cell. After 20 min equilibration, pyranine was added to the D compartment, the laser was activated at a frequency of 0.5 Hz and the electric signals were recorded. After accumulation of the data signals, NaCl (or KCl) was added to both compartments and signals were gathered again. All signals were corrected for the background noise emitted by the discharge of the flash lamps of the Yag laser.

The numeric simulation was carried out on a Silicon Graphics work station (Indigo). The differential equations and supporting program are available upon request.

3. Results

3.1. The electric signal of monensin mediated H^+/Na^+ exchange

The experimental system consists of three elements (see Scheme 3): A black lipid membrane which separates two troughs, perturbing laser pulse which upsets the system out of equilibrium and a current/voltage amplifier that records the capacitance current in the measuring circuit.

The laser pulse excites the pyranine (8-hydroxypyrene 1,3,6-trisulfonate), present on one side of the membrane, to its first electronic singlet state, causing

it to eject its hydroxyl proton [11]. As a result the dye side of the membrane is momentarily acidified [12]. The protonation of the membrane causes a charging of the membrane's capacitor. Due to the high resistance of the membrane ($\approx 1\ G\Omega$), the charge imbalance drives a capacitance current through the low impedance measuring circuit made of the conducting electrolytes, Pt electrode and amplifier. This current, picked up by the amplifier, is our experimental trace.

Pyranine has a marked affinity to phosphatidylcholine and is readily adsorbed to such membranes. Photo excitation of the adsorbed dye releases a proton to the bulk and the surface is charged by the adsorbed anion. To avoid this adsorption, the membrane was made of a mixture of phosphatidylcholine and phosphatidylserine on which the dye does not adsorb. Upon excitation of this system, net protonation of the surface takes place (for detail see Ref. [12]).

The electric signal associated with one face protonation of a black lipid membrane made of PC + PS (3:2) is shown in the inset to Fig. 1. Equilibration of the membrane by monensin has no effect on the recorded transient. The content of monensin in the membrane is rather small. As detailed in the following publication [13], it is only 5% of the PS content and the PS is 40% of the membrane headgroups. Thus the introduction of such a small increment of proton binding sites has a negligible effect on the electric signal.

Upon addition of transportable cations such as Na^+ or K^+, the electric signal is markedly changed. A typical current transient, measured in the presence of 70 mM NaCl, 20 μM monensin and pyranine (150 μM) is shown in Fig. 1. The tracing commences with a sharp positive spike (A) which is poorly resolved in time. Immediately afterwards we observe a sharp negative current transient (B) that continues to a broad positive wave (C), which is followed by a long negative one (D) until it fades to zero current after about 150 μs.

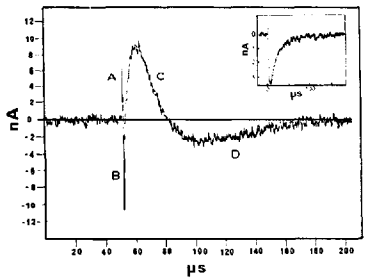

Fig. 1. Time-resolved current transient generated by a synchronized H^+/Na^+ exchange, carried out by monensin impregnated in black lipid membrane. A black lipid membrane made of phosphatidylserine plus phosphatidylcholine (2:3) was equilibrated with monensin (20 μM) and NaCl (70 mM) was added on both sides. Pyranine (150 μM) was present on one side only. The dye was excited by laser pulses ($\lambda = 355$ nm, 2 ns FWHM, ≈ 0.25 mJ/pulse). The current flowing through the external measuring circuit (see Scheme 3) was digitized, stored and averaged for 256 successive pulses. For the meaning of the letters on the figure, please see the text. (Inset) Capacitance current measured under comparable conditions in the absence of monensin and Na^+.

3.2. The effect of cation concentration on the current signal

The shape and magnitude of the current transient are functions of the ions present in the solution.

Fig. 2 depicts the results of a series of measurements, all carried out with the same membrane, where the concentrations of Na^+ (on both sides of the membrane) were gradually increased from 10 mM up to 210 mM. These tracings, which are the basis of the analysis that follows, are shown in the figure without the unresolved positive spike.

At low Na^+ concentration the measured signals are small and rather simple in shape. At higher Na^+ concentrations, the signal increases in amplitude and in complexity. Above approx. 200 mM the shape of the signal is invariant yet the amplitudes tend to decrease a little.

The same general features are seen when K^+ is used as the transportable cation. Fig. 3 depicts the current transients measured in the presence of 90 mM KCl. The transient current measurements were carried out with varying K^+ concentrations from 10 mM up to ≈ 330 mM. Above that the signals became independent of the cation concentrations (not shown).

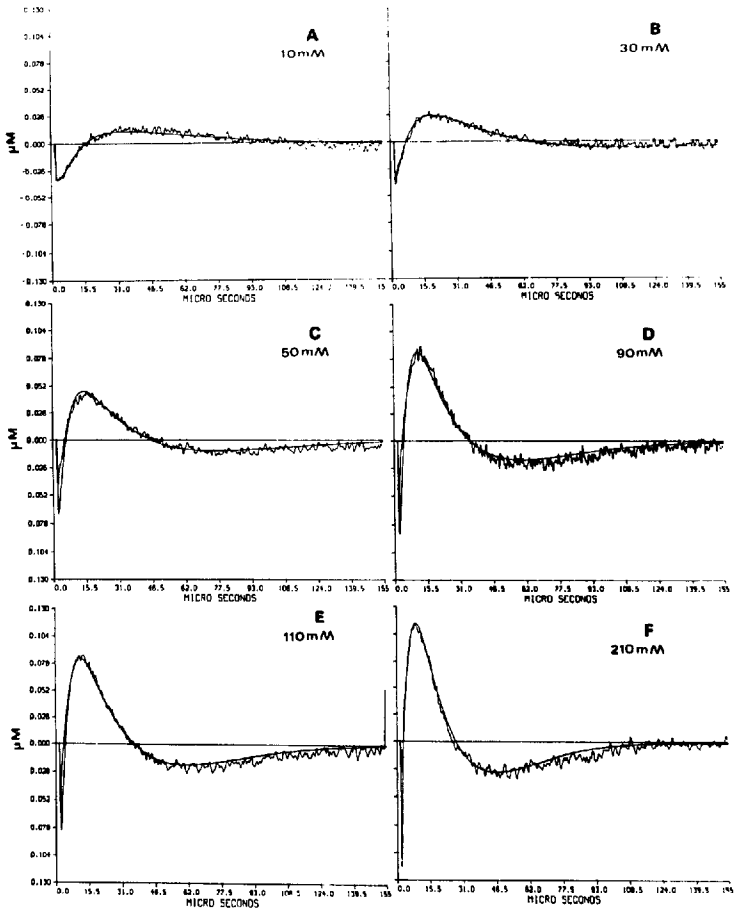
A
10mM
B
30mM
C
50mM
D
90mM
E
110mM
F
210mM
µM
MICRO SECONDS

Table 1
Kinetics and thermodynamic parameters characterizing the reaction of membrane-bound monensin with ions in the bulk phase

Chemical reaction		Rate const. [a]	Na^+–H^+	K^+–H^+
Binding of proton				
$\phi O^- + H^+$		k_1 [b]	$8.5 \cdot 10^{10}$	$8.5 \cdot 10^{10}$
$MoM + H^+$		k_3	$1.0 \cdot 10^{10}$	$0.7 \cdot 10^{10}$
$Mo^- + H^+$		k_7	$1.0 \cdot 10^{10}$	$1.0 \cdot 10^{10}$
$Ps^- + H^+$		k_{11} [b]	$1.0 \cdot 10^{10}$	$1.0 \cdot 10^{10}$
Surface-bulk proton transfer				
$PsH + \phi O^-$		k_{33} [b]	$1.0 \cdot 10^{10}$ [c]	$1.0 \cdot 10^{10}$
$MoH + \phi O^-$		k_{31}	$1.2 \cdot 10^{9}$ [c]	$1.2 \cdot 10^{9}$
Proton exchange on surface				
$MoMH^+ + Mo^-$		k_{39}	$3.0 \cdot 10^{10}$	$3.5 \cdot 10^{10}$
$PsH + MoM$		k_{38}	$0.8 \cdot 10^{10}$	$4.0 \cdot 10^{10}$
$Mo^- + PsH$		k_{36}	$0.3 \cdot 10^{10}$ [c]	$0.3 \cdot 10^{10}$
Dissociation of M^+				
$MoMH^+ \rightarrow MoH + M^+$		k_5	33 ns	0.5 ns
$MoM \rightarrow Mo^- + M^+$		k_{10}	25 ms	3 ms
Flux of neutral complexes				
MoH		k_{20}	$3.0 \cdot 10^{5}$	$2.2 \cdot 10^{5}$
MoM		k_{22}	$6.0 \cdot 10^{4}$	$5.0 \cdot 10^{4}$
Stability constants				
pK_{21}	$(\phi O^- + H^+)$		7.70	7.70
pK_{43}	$(MoNa + H^+)$		4.90	4.90
pK_{65}	$(MoH + Na^+)$		1.00	0.1
pK_{87}	$(Mo^- + H^+)$		6.62	6.62
pK_{109}	$(MoH + Na^+)$		2.7	1.8
pK_{1211}	$(PS^- + H^+)$		4.60	4.60

[a] The accuracy of the rate constant values is better than ± 10%.
[b] These rate constants had been determined before [7,11,12,14] and were not adjusted during the simulations.
[c] These values have been redetermined and differ by one order of magnitude or more from those of Gutman and Nachliel [7].

3.3. Kinetic analysis of the current transients

The multiple reversal of the current polarities, combined with their wide range of time constants and amplitudes, practically negate any attempts to describe the observed signals by a curve fitting expression. What is more, such a description will only be a graphical reproduction of the observation, not a mechanistic explanation.

To gain the desired understanding of the mechanism, we expressed all events as a sum of well defined chemical reactions (see Scheme 2), introduced a chemical perturbation to the system by incremental dissociation of the pyranine and propagated the perturbed equilibria in time so as to duplicate the response of the system to a specific (ΔH^+) perturbation. According to this model, the reactants are equally distributed on both sides of the membrane except for the dye (ΦOH) which is present exclusively on the D side. The reactants are in equilibrium with each other

Fig. 2. The effect of Na^+ concentration on shape and magnitude of the current transients generated by pulse acidification of one face of a black lipid membrane impregnated with monensin. The experimental curves were measured, as described in Fig. 1, in the presence of the NaCl concentrations as marked on each frame. The continuous lines superpositioned over the noise envelope of the experimental curves were generated for the given Na^+ concentration by numerical solution of the differential rate equations pertinent to the reactions defined in Scheme 2 with the rate constants listed in Table 1, Column 2 (Spike A (see Fig. 1) is omitted from all curves).

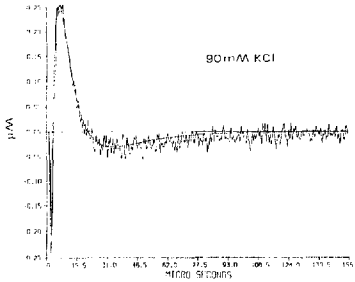

Fig. 3. Typical current transients measured with 90 mM KCl. The continuous line is the reconstructed dynamics generated by numeric integration of the differential rate equations using the rate constants listed in Table 1, Column 3 (Spike A (see Fig. 1) is omitted).

and, through the diffusion of the uncharged monensin compounds MoH and MoNa (or MoK), matter can be transferred across the membrane.

To attain the mathematical expression for the perturbation, all equilibria were converted into differential rate equations which comply with the detailed balance principle [7]. These equations consist of a set of 11 coupled, non linear differential rate equations, where both rates and concentrations may be treated as adjustable parameters. The various rate constants are interrelated by their equilibrium constants.

The simulation procedure is based on assigning discrete values to the adjustable parameter and integration of the equations over time. The difference between the electric charge transients on each side of the membrane (dQ_D/dt) and (dQ_R/dt) were calculated to obtain the total charge disbalance transient (dQ_T/dt), which represents the capacitance current as it varies with time. The solution to the system will be the combination of rate constants which reproduces all recorded transients measured with a given cation (either Na^+ or K^+), regardless of the ion concentration. The requirement that the same set will reproduce the dynamics recorded from subsaturating up to saturating ion concentrations increased the accuracy of the analysis. On the basis of these results we amended some previously reported rate constants [7]. The solution of the dynamics is represented by the simulated curves shown in Figs. 2, 3 and 5 (Frame F). Each experimental curve in these figures is drawn together with a theoretical fitted curve that employs the same rate constants. The rate constants that solve the Na^+ and K^+ systems are listed in Table 1. Altogether the values given in Table 1 were compiled from the fitting of more than 40 independent experiments carried out with varying concentrations of either K^+ or Na^+ as transportable ions.

Comparison of the rate constants measured with the two cations reveals that for those reactions where Na^+ or K^+ are not participating reactants (bold face numbers), the rate constants are identical for the two systems.

The rate constants (listed in Table 1) accurately retrace the experimental signal within the electronic noise envelope. Any deviation from the given values causes the simulated curve to deviate from the experimental one in a way that cannot be ameliorated by changing one or even all other rate constants.

The rigorousness of the simulation was tested by varying each of the parameters and checking to what extent the resulting curve will deviate from the experimental one. This test is demonstrated in Fig. 4, where we used the experimental curve shown in Fig.

Fig. 4. The stiffness of the numerical simulations. In each frame of this figure we modulate the magnitude of one adjustable parameter within the margin defined in the frame. The three theoretical curves shown in the frames correspond with: (————) the lower value of the parameter; (- - -) mid value of the range (also taken as best fit) and (— - —) the upper value of the adjustable parameter. All curves are presented with the transient current measured with 70 mM NaCl as shown in Fig. 1, excluding the poorly resolved 'A' spike. The variables appearing in the frames are: (A) The equilibrium constant for binding of H^+ to MoNa (reaction 4 in Scheme 2). (B) The equilibrium constant of the ternary complex for dissociation to MoH and Na^+ (reaction 10 in Scheme 2). (C) The equilibrium constant of Mo^- protonation (reaction 3 in Scheme 2). (D) Rate constant of proton transfer from PSH to Mo^- (forward rate in reaction 5, Scheme 2). (E) Rate of MoH flux across the membrane (reaction 12 in Scheme 2). (F) Rate of MoNa flux across the membrane (reaction 13 in Scheme 2).

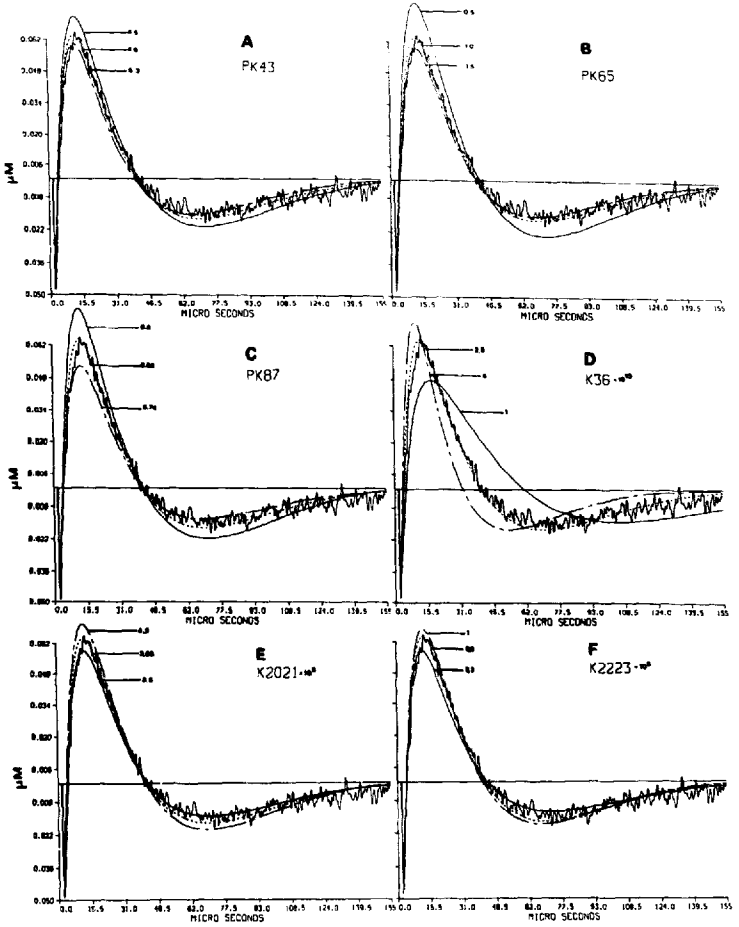
A
PK43
B
PK65
C
PK87
D
E
K2021
F
K2223
μM
MICRO SECONDS

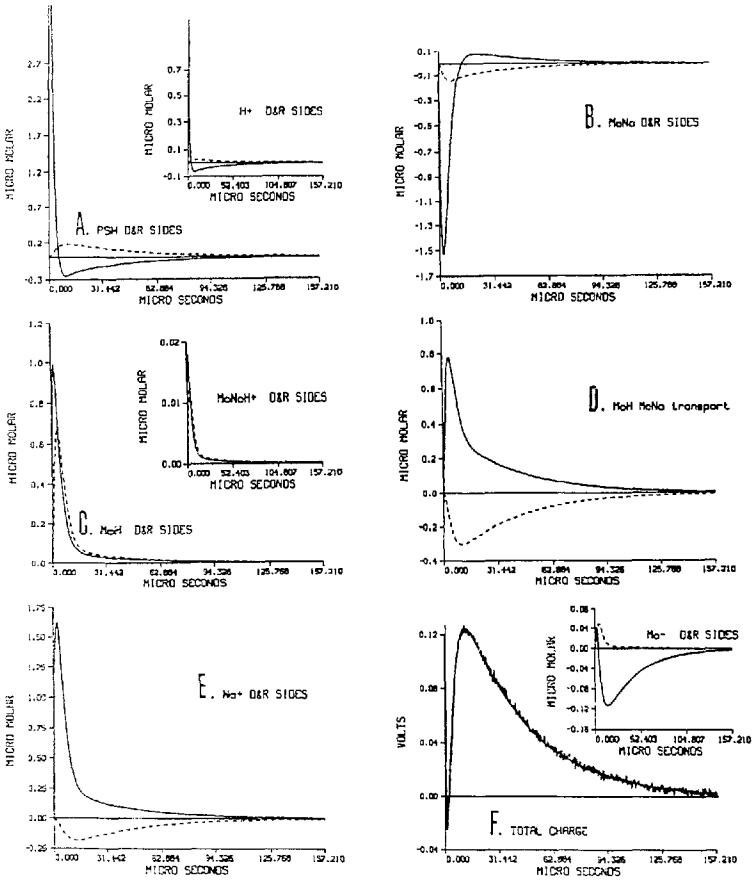
A. PSH D&R SIDES
H+ D&R SIDES
B. MoNa D&R SIDES
C. MoH D&R SIDES
MoNoH+ D&R SIDES
D. MoH MoNa transport
E. Na+ D&R SIDES
F. TOTAL CHARGE
Na+ D&R SIDES
MICRO MOLAR
MICRO SECONDS
VOLTS

I as a reference curve. In each frame of the figure one parameter was varied, above and below the optimal value. For the sake of brevity we present only those reactions where the ionophore is a reactant, yet it should be emphasized that the rates of all other reactions, like protonation of PS^- or the reaction of ϕO^- with PSH, also affect the dynamics.

Frames A, B and C demonstrate the sensitivity of the simulation to variation in equilibrium constants. Changes as small as 0.5 log unit or even less (Frame C) already distort the curve well beyond the electronic noise.

The effects of rate constants on the simulations are shown in Frames D, E and F. The protonation of the monensin, via proton transfer from the carboxylate of the phosphatidylserine is a very crucial parameter. Very small variations in its value suffice to offset the dynamics out of the noise envelope (Frame D). Finally the diffusion rates of the neutral species (MoH and MoNa) distort the dynamics when their rate varies by as little as ±10% (Frames E and F).

4. Discussion

4.1. Quantitation of charge displacement

The simulated dynamics detailed in Fig. 5 utilize concentration units for quantitation of transients. It is of interest to convert these numbers to the number of translocated charges. For that purpose we have to define the volume of the reaction space. The excitation beam, as focused on the membrane, irradiates an area of about $3.1 \cdot 10^{-4}$ cm^2. The depth of the reaction layer is approximated as the distance that a free proton will diffuse within the lifetime of the free proton increment (see Fig. 5A), which is approx. 10 μs. The corresponding width of the layer will be $l = \sqrt{(2\,Dt)} = 4 \cdot 10^{-5}$ cm. That makes the volume of the reaction space $\approx 1.3 \cdot 10^{-11}$ liter. Multiplication of that volume by the molar increment of charges yields the number of charges associated with the electric perturbation to be $\approx 1 \cdot 10^{-18}$ mol or $\approx 7 \cdot 10^5$ electronic charges. This value is surprisingly small and calls for corroboration by the measured electric parameters.

Integration of current over the time of the experimental signal (as in Fig. 1) yields a maximal increment of $1.5 \cdot 10^{-13}$ C which corresponds with $9 \cdot 10^5$ electron charges. Recent measurements by Bransburg-Zabary et al. [13] that utilized a 60 dB voltage amplifier, recorded the voltage built up on the membrane capacitor (Fig. 5, Frame F). The measured voltage, 60 μV and the membrane capacitance (2 nF) corresponds with $\approx 10^6$ electron charges associated with the observed transient. Thus direct measurements and the simulation are in agreement about the magnitude of the perturbation. It is of interest to point out the extreme sensitivity of the electric measurements, which provide time-resolved dynamics with high signal/noise ratio while the actual transient is as small as 10^{-18} mol.

4.2. The uniqueness of the simulation

The numeric simulation reproduces the amplitude and shape of a multiphasic transient by a set of 11 coupled differential equations. By these equations

Fig. 5. Molecular scenario of the synchronized H^+/Na^+ exchange by monensin in a black lipid membrane. Each frame in the figure describes the dynamics of a single reactant both on the D side (————) and R side (- - -) of the membrane. The scenario corresponds with measurements carried out in the presence of 170 mM NaCl and followed up by 60 dB 30 MHz voltage amplifier [13]. The simulated curves are based on the rate constants listed in Table 1. Frame A: Protonation of the phosphoserine headgroups. (Inset A) The free proton concentration in the bulk phase. Note that the D side of the membrane undergoes transient alkalinization while the R side exhibits an extended phase of acidification. Frame B: Decrement of MoNa. Notice that the D face tracing exhibits two phases. The first one is immediate depletion coupled with $MoNaH^+$ formation. The second one, appearing as an incremental concentration, corresponds with influx of MoNa from the R side. Frame C: Incremental concentration of MoH. Note the 100-fold change in order of magnitude of the abscissa with respect to the inset. (Inset C) Dynamics of the ternary complex $MoNaH^+$. Frame D: The flux of the neutral species across the membrane. The upper curve (solid line) depicts the flux of MoH from D to R side, while the negative tracing (dashed line) depicts the reverse flux of MoNa from R face to the D one. Frame E: The incremental concentration of Na^+ discharged from the membrane to the bulk. Frame F: The net polarization of the membrane. The computed curve is shown together with the experimental voltage transient. (Inset F) The dynamics of Mo^- accumulation on the D and R faces of the membrane.

and a single set of rate constants we simulated more than 40 experimental curves whose size and shape varied in correspondence with the saturation of the monensin by either Na^+ or K^+. As demonstrated in Fig. 4, the reconstruction of a single experiment falls within a very narrow range of variance for each of the adjustable parameters. The simultaneous fitting of two families of curves (one for Na^+, the other for K^+) with identical values for the rate constants in which the metal ion is not involved (bold face numbers in Table 1), represents, in our experience, a unique solution of the system.

The capacity of the numeric simulation to reproduce all experimental curves can be used as a tool for understanding the role of the partial reactions in the generation of the overall electric transient.

4.3. The mechanism of the reaction

The model given in Scheme 2 is maximalistic, defining each possible reaction by its rate and equilibrium constants. The multiplicity of parallel reactions prohibits any attempt to describe the observed transient as a set of sequential events. The understanding of the origin of electric transient is based on the numerical procedure which calculates the role of each reactant in the overall process. Based on the computed dynamics of the individual reactants, we can reconstruct the whole process.

Fig. 5 is a breakdown of the electric transient, measured with 170 mM NaCl, to depict the dynamics of each component of the system. Reactants which are present on the driving side (D) of the membrane are depicted by a solid line, while those on the opposite face of the membrane (R) are shown by a dashed line. The reactions which dominate the dynamics of the reactant are identified as numbered in Scheme 2.

The primary event of the transient is the photodissociation of the pyranine by the laser pulse. The protons and ΦO^- anion, generated in equal quantities by the photodissociation, mostly recombine with each other (reaction 1) (see the inset to Fig. 5, Frame A). Yet at a certain time the free proton concentration on D side declines below the prepulse level, indicating that some of the perturbation propagated across the membrane.

The first step leading to the disbalance between the two faces is the massive protonation of the carboxylates of phosphatidylserine which are on the D face of the membrane (reaction 2; see Frame A). The protonation itself, which is an unresolved submicrosecond event [7], is followed by a rapid phase where protons are lost from the carboxylates, up to a point where the net alkalinization of the phosphoserine headgroups takes place (Frame A). This apparent proton deficit implies that the protons had been transferred from PSH to the monensin metal complex, as defined by reaction 6. (It is of interest to point out that the rate of proton transfer from phosphoserine to monensin anion (Mo^-) (reaction 5) is faster than the rate of reaction 6. Yet at any Na^+ concentration which is higher than the dissociation constant of MoNa complex (a few mM), the abundance of Mo^- is negligible and has a vanishing contribution to the dynamics.

The fast protonation of MoNa by PSH (reaction 6) leads to depletion of the MoNa population on the D side (see Frame B) and in parallel the ternary complex concentration increases (inset to Frame C). Comparison of the increments of MoH (Frame C) versus $MoNaH^+$ reveals a wide discrepancy between the reactants concentration, which originates from the transient nature of the ternary complex [6]. The $MoNaH^+$ is a short lifetime complex that dissociates with a time constant of approx. 30 ns (reaction 10), ejecting Na^+ to the aqueous phase and enriching the MoH population on the D side. The appearance of MoH on the D face and in parallel the depletion of MoNa (Frame B) creates a concentration gradient for both MoH and MoNa between the D and R sides of the membrane. MoH diffuses from D towards R (reaction 12, Frame D, upper solid curve) while MoNa flows in the opposite direction (reaction 13, Frame D, dashed line).

The flux of MoH to the R side of the membrane is an import of acidic species which charges, via reaction 5, the PS^- on the R side (see Frame A, dashed line). Both MoH and the protonated phosphoserine dissociate (reactions nos. 2 and 3), causing transient acidification of the R side bulk (see inset to Frame A, dashed line).

The influx of MoH to the R side and the parallel depletion of MoNa (Frame B, dashed line) by a flux towards the D side (Frame D, dashed line) upset the bulk-surface ionic equilibria on the R side (by reactions 7,10 and 11, all linked in a thermodynamic box)

and Na^+ ions are taken up from the solution (Frame E, dashed line). This sequence of reactions is the manifestation of the steady state H^+/Na^+ exchange in the time-resolved domain.

The outcome of the reactions proceeding on both sides of the membrane and the flux of uncharged species across the membrane are a transient transport of Na^+ from R to D compartment and imbalance of Mo^- concentration between the two faces. Mo^- appears on the R face (inset to Frame F, dashed line) and causes negative charging of this face of the membrane. On the D side the Mo^- transient is more complex (inset to Frame F, solid line), but its most prominent feature is decrement below the equilibrium level, i.e. the D face gains a positive charge.

The summation of all calculated charges, on both sides of the membrane, is shown in frame F. This transient is presented together with experimentally measured voltage recording [13]. The fitting of the theoretical transient with the experimental curve is as good as that obtained with the current amplifier (see Figs. 2 and 3).

4.4. Quantitative evaluation of the rate constants

The rate constants given in Table 1 are grouped by the nature of the reaction. In the first group we listed the reactions where the free diffusing proton is one of the reactants. The magnitude of the rates, compatible with those of diffusion controlled reaction [14], indicates that the proton binding sites of the reactants are well exposed to the bulk. The reactivity of protonated surface moieties with ΦO^- (see second group in Table 1) are also compatible with the diffusion controlled reaction between the water soluble anion and well exposed sites.

The third group lists the rates of proton exchange reactions among adjacent moieties on the surface, rates which are extremely sensitive to the distance between the reactants [15]. Examination of their value reveals a great difference between the rates of proton transfer from PSH to the two Me-monensin complexes. The rate of reaction with MoK, which is about 5-times faster than with MoNa, may point to unequal orientations of the two metal-ionophore complexes with respect to the membrane's surface.

The next group of parameters, as listed in Table 1, are the dissociation time constants of the metal ions from their monensin complexes. The MoNa complex has a time constant which is about 10-times longer than that of the respective K^+ complex, which is in accord with the wellknown stabilities of these complexes [1,5,16]. Yet we must indicate that these time constants are slower by orders of magnitude with respect to the dissociation of cations from the ternary complexes. Thus even a minor fraction of a ternary complex, in equilibrium with MoM species, will provide the 'kinetically favoured pathway' for dissociation of the metallic ion from monensin.

4.5. The selectivity of monensin

Monensin is known for long to prefer Na^+ over K^+ as transported cations [1]. The selectivity was traditionally ascribed to the higher stability of the MoNa complex. The stability of the complexes was measured in organic solvent [6], calculated by molecular dynamics evaluation of the stability of the crystalline structure [4], deduced from kinetic analysis of time-resolved measurements [5] and reconfirmed by our experiments (Table 1). Yet, as emerges from our global analysis, the selectivity is not only a matter of affinity but also of diffusivity. There is a large difference between the rate of passage of the three uncharged species. MoH crosses the membrane with time constant $\tau = 2.8$ μs, while the Na^+ and K^+ complexes have time constants of 16 μs and 200 μs, respectively. These unequal first passage times provide a sharp tool for probing the membrane–ionophore interactions.

4.6. Quantitative evaluation of the MoH mobility in the membrane

The three uncharged complexes have a comparable molecular weight and their external dimensions, as gathered from X-ray diffraction of crystals, are also quite similar [2–4]. Thus the large difference in passage time must be attributed to the electric properties of the complexes.

The MoH complex differs from the metal ion ones by the fact that the proton does not occupy the central position of the ionophore but reacts directly with the C_1 carboxylate. As a result MoH is not only neutral but also devoid of a dipole moment. For this reason we can assume that the only drag which restricts the

passage of MoH is the viscosity of the membrane. Approximating MoH as a sphere with a radius of approx. 5 Å, its diffusion coefficient in a membrane, having a viscosity of about 1 P [17], will be $D \approx 3.7 \cdot 10^{-8}$ cm^2/s. Such particles will move across the membrane with a first passage time of $t = l^2/2D =$ 2.5–3 μs, which is in accord with our experimental observation.

4.7. The passage of MoNa and MoK

The first passage times for the metal ionophore complexes are significantly longer than that of MoH, indicating that besides the viscous drag there is another force operating on these complexes. We attribute their slower migration to the interaction of their dipoles with the membrane's electric field, generated by the orientation of both the carbonyls of the *sn*-2 chain [8] and the water of the hydration layer [9]. The magnitude of the dipolar field (positive inside) as measured by the distribution of hydrophobic ions is about 230 mV, of which approx. 120 mV are contributed by the ordered water at the interface [9].

The energy of interaction between the complex and the dipolar field can be equated with the excess of activation energy as derived for MoNa transport with respect to that of MoH.

$$E_a(\text{MoNa}) = -RT \ln(k_{22}/k_{20}) = 0.96 \; kcal/mol$$

For a field of 230 mV falling within a span of approx. 10 Å [18], and the measured activation energy of 1 kcal/mol corresponds with dipole moment of 8.6 Debye units. The dipole moment of MoNa, estimated from the distance between Na^+ and the nearest atom of the carboxylate, as based on the crystal structure of MoNa · $2H_2O$, is $p < 13$ *D*. Thus we conclude that the reduced mobility of MoNa, with respect to MoH, is explainable by the dipole of MoNa as estimated from its crystalline configuration. This assignment is in accord with the measurements of Turner [10] that confirmed the solution structure of MoNa (in chloroform) to be identical with the crystal structure of the complex.

The excess activation energy for MoK passage is much larger.

$$E_a(\text{MoK}) = -RT \ln(k_{22}/k_{20}) = 2.5 \; kcal/mol$$

To attain such a value the dipole of MoK should be $p = 22.6$ *D* which is larger than the maximal dipole $p < 17.4$ *D* as calculated from the crystalline configuration of MoK · $2H_2O$.

The apparent discrepancy between the measured dipole and the predicted one indicates that the crystal structure is not maintained at the membrane water junction. The membrane water interface is a complex environment, characterized by steep gradients of the dielectric constant, the availability of water and the electric field. Apparently it can modulate the structure of solutes embedded in this layer.

4.8. Concluding remarks

In the present study we exploited the proton pulse technique for measuring the motion of ions across black lipid membrane in the time-resolved domain. The high time resolution allowed us to break the electrosilence of cation-proton antiport by the mere advantage of looking at the molecular events in their own time scale and synchronizing their reaction by an external perturbation.

These results, supported by rigorous analytic methods, could reveal some of the inner structure of the water/membrane interface and point to the fact that compounds within this region may assume configurations not common to their aqueous or crystalline ones. As will be shown in the following publication [13], this system was successfully implemented for detecting microheterogeneities of the membrane upon incorporation of cholesterol.

Acknowledgements

This research was supported by research grants from the Office of Naval Research, NOOO14-94-0533 and the United States–Israel Binational Science Foundation (91-00226). The authors are grateful to S. Bransburg-Zabary for her permission to use one of the figures from her M.Sc. thesis.

References

[1] Pressman, B.C. (1968) Fed. Proc. 27, 1283–1288.
[2] Pinkerton, M. and Steinrauf, L.K. (1970) J. Mol. Biol. 49, 533–546.

[3] Duax, W.L., Smith, G.D. and Strong, P.D. (1980) J. Am. Chem. Soc. 102, 6725–6729.
[4] Pangborn, W., Duax, W. and Langs, D. (1987) J. Am. Chem. Soc. 109, 2163–2165.
[5] Prabhananda, B.S. and Kombrabail, M.H. (1992) Biochim. Biophys. Acta 1106, 171–177.
[6] Cox, B.G., Firman, P. and Schneider, H. (1985) J. Am. Chem. Soc. 107, 4297–4300.
[7] Gutman, M. and Nachliel, E. (1989) Electrochim. Acta 34, 1801–1805.
[8] Flewelling, F. and Hubbell, W.L. (1986) Biophys. J. 49, 541–552.
[9] Gawrisch, K., Ruston, D., Zimmemberg, J., Parsegian, V.A., Rand, R.P. and Fuller, N. (1992) Biophys. J. 61, 1213–1223.
[10] Turner, D.L. (1995) J. Magn. Reson. 108, 137–142.
[11] Gutman, M. (1984) Methods Biochem. Anal. 30, 1–103.
[12] Gutman, M., Nachliel, E., Bamberg, E. and Christensen, B. (1987) Biochim. Biophys. Acta 905, 390–398.
[13] Bransburg-Zabary, S., Nachliel, E. and Gutman, M. (1996) Biochim. Biophys. Acta 1285, 146–154.
[14] Gutman, M. and Nachliel, E. (1990) Biochim. Biophys. Acta 1015, 391–414.
[15] Gutman, M. and Nachliel, E. (1995) Biochim. Biophys. Acta 1231, 123–138.
[16] Cox, B.G., Van Truyg, N. Rzeszotarska, J. and Schneider, H. (1984) J. Am. Chem. Soc. 106, 5965–5969.
[17] Jain, M.K. and Wagner, R.C. (1980) Introduction to Biological Membranes, Wiley, New York.
[18] Marrink, S.-J., Berkowitz, M. and Berendsen, H.J.C. (1993) Langmuir 9, 3122–3131.